Impact of DFT-Based Phasor Estimation Errors Due to Commutation Failures of LCC-HVDC Links on the Protection of AC Lines in the Near Vicinity

Kleber M. Silva, José Jorge C. Tavares, Nilo Sérgio S. Ribeiro, Felipe V. Lopes

***Abstract*—Commutation failure (CF) is an inherent issue for Line-Commutated Converter (LCC) HVDC technology. Whenever it happens, voltage and current waveforms throughout the AC system in the near vicinity of LCC-HVDC links become quite distorted. In this paper, it is assessed the impact of such kind of distortion on transient response of phasor estimation algorithms and, in turn, on the performance of AC transmission lines protection. Different discrete Fourier transform (DFT) based algorithms are implemented, and distance, differential and directional protection functions are evaluated. The obtained results reveal that phasor estimation errors arise whenever CFs take place, which may lead protection functions to misoperate, such that false trip command may be issued for external faults.**

***Keywords*—LCC-HVDC system, commutation failures, phasor estimation, DFT-based algorithms, transmission lines protection.**

I. Introduction

THE increasing load demand has required power systems evolve to huge interconnected systems spanning entire countries. Often load centers are very far from the main generation plants, requiring bulk power transmission over very long distances. Among the feasible solutions, the LCC-HVDC technology is the most widespread [1]. However, CF is a common issue in the operation of this kind of solution. It mainly occurs as a consequence of voltage dips due to AC system faults or switching maneuvers nearby the inverter station. In systems with high level of HVDC penetration, the multi-infeed phenomena increases CFs frequency of occurrence even more [2]. One of the consequences of CF is a momentary interruption of power transmission through the link, leading the disturbance to be aggravated. Furthermore, voltage and current waveforms in nearby AC systems become quite distorted due to the presence of components with a wide range of frequencies, requiring a proper filtering process before protection functions are applied [3].

The distance protection (ANSI Code 21) of AC lines in the near vicinity of LCC-HVDC was evaluated in [4]–[6], whereas line differential protection (ANSI Code 87L) and directional overcurrent protection (ANSI Code 67) were evaluated in [7] and [8], respectively. These works focused on the analysis of the impact of CFs on the protection dependability, which is a major concern for weak systems. Nevertheless, they did not addressed protection security issues that may arise depending on the impact of CFs on phasor estimation.

Phasor estimation process plays a major role in modern numerical relays [9]. The algorithms must provide bandpass response about the fundamental frequency, good transient behavior, harmonic elimination and decaying dc component rejection as well. Most of them are modifications of the traditional full-cycle DFT (FCDFT) and half-cycle DFT (HCDFT) algorithms [10]–[21]. Their overall performances are usually quite good, such that DFT-based algorithms have been widely used in protection relays available on the market. However, to prevent misoperation of AC equipment protection, it is of utmost importance to analyze their performance for critical system operation conditions, such as during successive CFs in LCC-HVDC links.

In this paper, the major contribution lies in assessing the impact of phasor estimation errors due to CFs of LCC-HVDC links on the nearby AC lines protection. Different DFT-based phasor estimation algorithms were implemented, thereby distance, differential, and directional protection performances were analyzed, focusing on security issues for external faults. The case study of the Brazilian Madeira River LCC-HVDC link is evaluated. The obtained results reveal that phasor estimation errors arise whenever CF takes place, and, in some cases, it may lead protection functions to misoperate, issuing false trip commands for external faults. Nevertheless, since distortions on AC voltage and current waveforms due to CFs are unpredictable, errors on phasor estimation are not known a priori, as well as their impact on protection functions. As a result, for the sake of security, according to the obtained results, it is recommend a more conservative approach on settings procedure, to avoid protection misoperation.

II. Power System Model

Fig. 1 depicts the power system evaluated in this paper, corresponding to the LCC-HVDC Madeira River link installed in Brazil, and the nearby AC system. The HVDC link is composed by two bipoles 2450 km long, with rated power of 3150 MW, $\pm$ 600 kV, which interconnect two stations, named Coletora Porto Velho (CPV) and Araraquara II (AQD) 500 kV. Each bipole was modelled using the Cigré Benchmark ATP/ATPDraw bipole model reported in [22], which is readily available in [23]. In this model, it is implemented the well-known voltage dependent current order limiters (VDCOL) control strategy, to prevent instability

Paper submitted to the International Conference on Power Systems Transients (IPST2021) in Belo Horizonte, Brazil June 6-10, 2021.

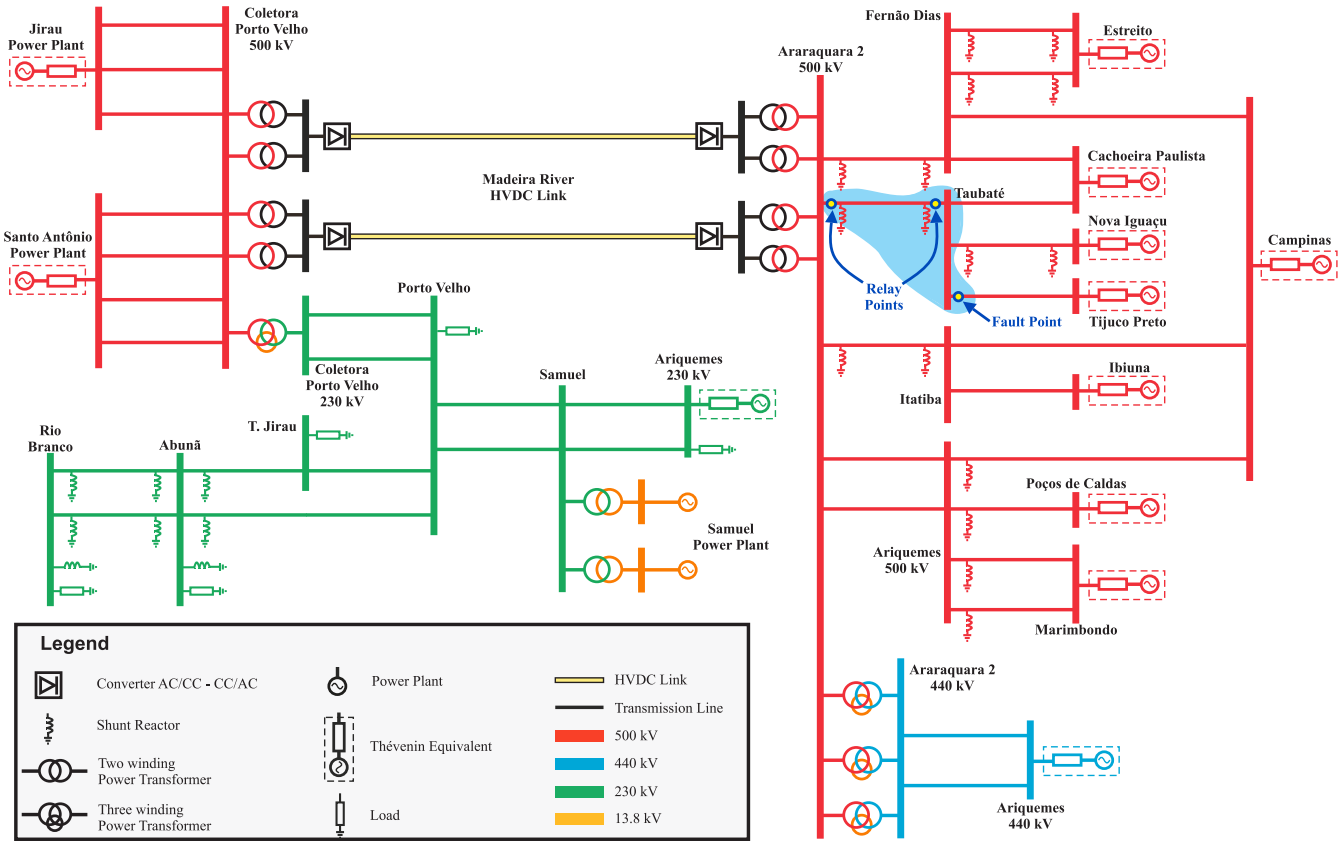

Fig. 1. Single-line diagram of the evaluated power system: the Brazilian LCC-HVDC Madeira River link and the nearby AC system.

in AC voltage and to mitigate successive CFs, by reducing the commutated DC current. In this paper, instead of using Thevenin equivalent in both rectifier and inverter stations as reported in [22], the AC system (60 Hz) in the vicinity of the HVDC link was modeled, using real data from the Brazilian power grid. Power transformers were represented using the saturable transfromer model, including their saturation curves [24]. Transmission lines were modeled as fully transposed lines using the Bergeron model, except the analyzed 500 kV line, 334 km long, between the stations AQD and Taubaté (TBT), which was modeled as a transposed line with the transposition scheme $1/6 - 1/3 - 1/3 - 1/6$, using the JMarti model [24]. Load and shunt reactors were modelled as lumped components. Thévenin's equivalents were included in AC boundary buses, considering both self and mutual impedances. Models for current transformers (CTs) and coupling capacitor voltage transformers (CCVTs) were also included in ATP/ATPDraw simulations at the relay points shown in Fig. 1 [25], [26].

III. Obtained Results and Analysis

Aiming to evaluate the impact of phasor estimation errors on the protection of AC lines in the near vicinity of LCC-HVDC links, different protection functions were assessed for the line between AQD and TBT stations depicted in Fig. 1. As aforementioned, the major concern lies on ensuring the protection security, such that several external faults at adjacent lines connected to TBT station were simulated. In particular, results for four solid fault cases are described in this paper: AG, BC, BCG and ABC near TBT station (see the fault point shown in Fig. 1). In this paper, half-cycle DFT-based algorithms reported in [21] and [17] (H1 and H2 algorithms, respectively) are evaluated. Furthermore, full-cycle DFT-based algorithms reported in [11] and [21] (F1 and F2 algorithms, respectively) are also evaluated. Nevertheless, it is noteworthy to point out that results discussed in this paper might happen with any other DFT-based algorithm.

Simulations were carried out in ATP/ATPDraw using time step of 1 μs. Then, a third order low-pass anti-aliasing Butterworth filter with cutoff frequency at 180 Hz was applied on the secondary voltages and currents obtained from CCVTs and CTs included at the relay points (see Fig. 1), respectively. The filtered signals were resampled at 16 samples per cycle of 60 Hz and then phasors were estimated using the DFT-based algorithms. Finally, the protection functions are evaluated, being the obtained results discussed.

A. CF Simulations

During CFs, a converter valve that is supposed to turn off continues to conduct, in such way that the current is not transferred to the next valve in the firing sequence [1]. To exemplify the impact that CFs may cause, Figs. 2(a) and 2(b) represent, respectively, the high-voltage winding currents of YY and YΔ converter transformers of the pole+ in the bipole 1. In this case, an external AG solid fault was simulated at the fault point shown in Fig. 1 from 65 ms.

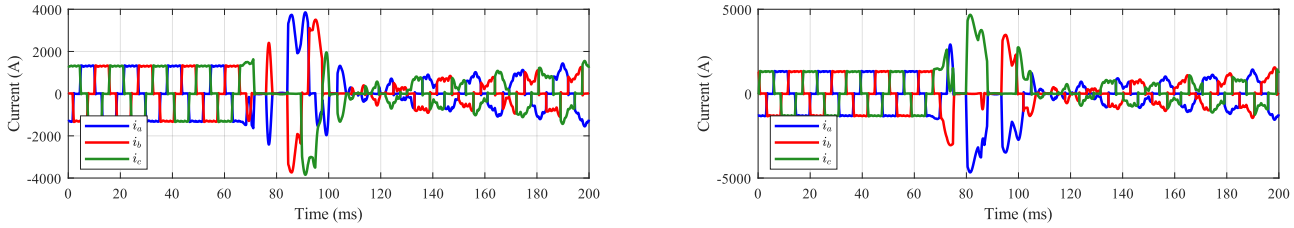

(a) (b)

Fig. 2. Simulated signals in the LCC-HVDC link during the external close-in solid AG fault: (a) high-voltage winding currents of the YY converter transformer related to the pole+ of the bipole 1; (b) high-voltage winding currents of the YΔ converter transformer related to the pole+ of the bipole 1.

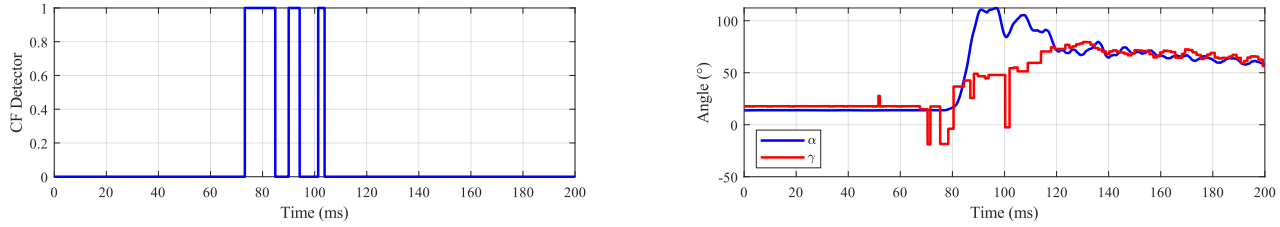

(a) (b)

Fig. 3. Simulated signals in the LCC-HVDC link during the external close-in solid AG fault: (a) CF detection logic implemented in the Cigré Benchmark HVDC model [22]; (b) the delay angle α and the extinction angle γ related to the bipole 1.

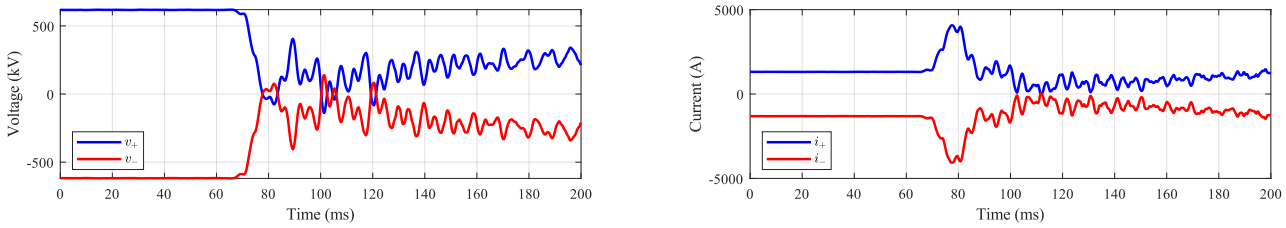

(a) (b)

Fig. 4. Simulated signals in the LCC-HVDC link during the external close-in solid AG fault: (a) Voltage at the inverter station of the bipole 1; (b) current at the inverter station of the bipole 1.

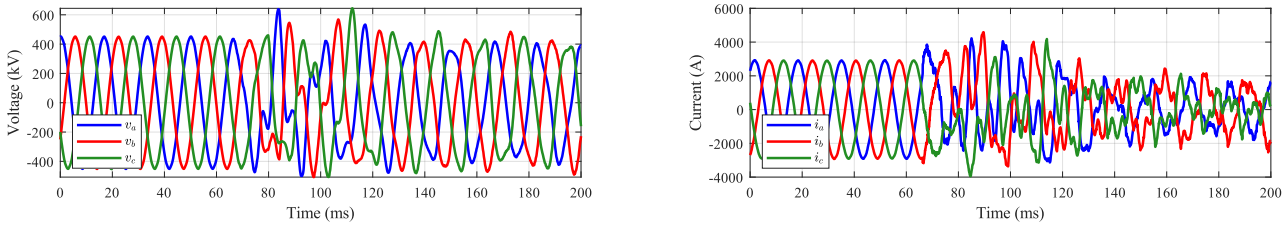

(a) (b)

Fig. 5. Simulated signals in the LCC-HVDC link during the external close-in solid AG fault: (a) voltage at AQD station; (b) infeed currents flowing out the bipole 1 toward AQD station.

In Fig. 3(a), it is depicted the CF detector implemented in the Cigré ATP/ATPDraw HVDC model [22], revealing time periods during which CF is detected. Furthermore, it can be seen in Fig. 3(b) that the delay angle α and the extinction angle γ suffer a large variation after the fault inception. As a consequence, DC voltage and currents [see Figs. 4(a) and 4(b)] becomes quite distorted, as well as the AC voltage at the AQD staion [see Fig. 5(a)] and AC currents flowing out the LCC-HVDC link [see Fig. 5(b)]. It is noteworthy that the behaviour of valves firing is unpredictable during CFs. Therefore, its impact on AC voltage and current waveforms and, in turn, in their frequency spectrum is not known a priory.

B. Errors on DFT-Based Phasor Estimation

Figs. 6(a) and 7(a) show, respectively, phasor magnitudes of voltage and current signals at the relay point in AQD station (see Fig. 1) during the same AG solid fault described in the previous Section, considering that the LCC-HVDC link is out of service and disconnected from AQD station. As one can see, both half-cycle and full-cycle DFT-based algorithms perform as expected, not presenting significant errors on phasor estimation, except the overshoot during the

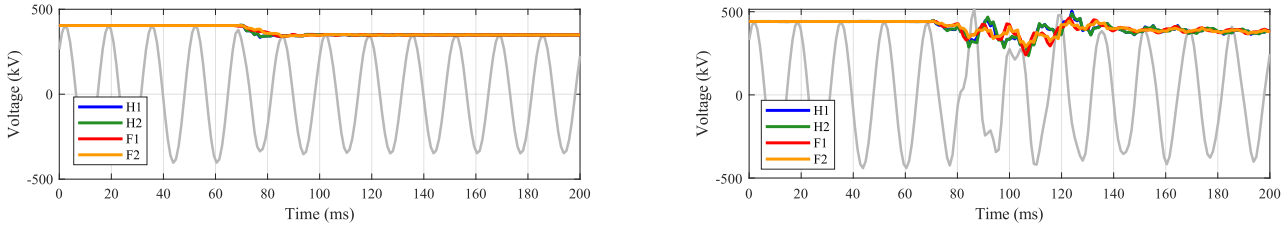

(a) (b)

Fig. 6. Magnitude of the voltage phasors simulated at the relay point in TBT station during the external close-in solid AG fault: (a) with the LCC-HVDC link disconnected from TBT station; (b) with the LCC-HVDC link connected to AQD station.

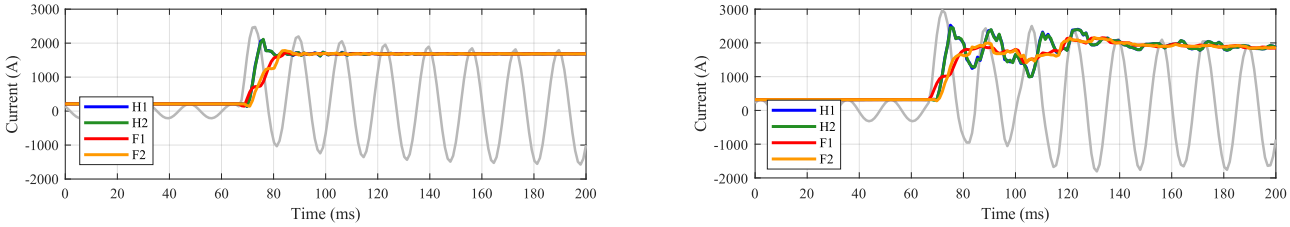

(a) (b)

Fig. 7. Magnitude of the current phasors simulated at the relay point in AQD station during the external close-in solid AG fault: (a) with the LCC-HVDC link disconnected from AQD station; (b) with the LCC-HVDC link connected to AQD station.

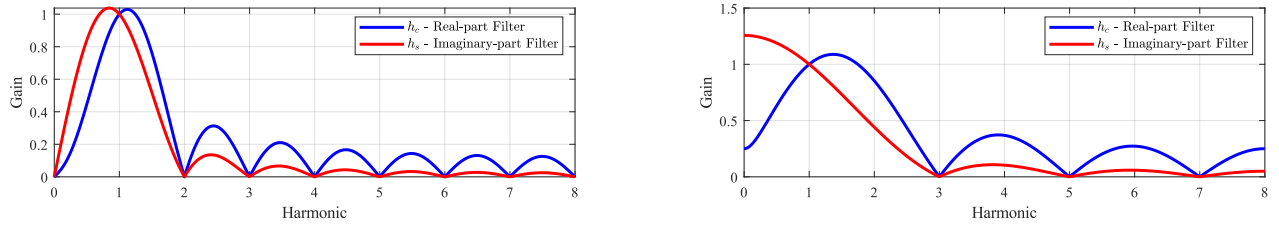

(a) (b)

Fig. 8. Frequency response magnitude of the traditional DFT filters: (a) FCDFT (b) HCDFT.

transient period caused by the decaying DC component effect. Conversely, Figs. 6(b) and 7(b) depict the phasor magnitudes for the same fault, but now considering that both bipoles of the LCC-HVDC link are in service and connected to AQD station. When the fault takes place at 65 ms, currents coming from the LCC-HVDC link add distortions on current signals measured at relay point, and cause errors in phasor estimation. One can see that voltage at the relay point are also affected by the LCC-HVDC link operation during AC system faults. Furthermore, it is clear that H1 and H2 algorithms are much more sensitive to those distorted waveforms than F1 and F2 algorithms. To better understand this result, one can analyze the frequency response of real- and imaginary-part filters of the traditional DFT algorithms shown in Figs. 8(a) and 8(b) [9]. Full-cycle filters reject all harmonics, but their frequency responses have side-lobes between harmonics, revealing interharmonics are not filtered out. Half-cycle filters, in turn, do not reject even harmonics and DC component, and their frequency responses have larger side-lobes than those of full-cycle filters, what results in larger errors on phasor estimation. It is noteworthy to point out that, even tough the frequency response of the evaluated DFT-based algorithms are not exactly equal to those of traditional FCDFT and HCDFT, these major characteristics are inherited.

C. Distance Protection Function

To assess the impact of LCC-HVDC link on distance protection during faults on the nearby AC system, it was considered a relay at AQD station, installed at the line AQD−TBT, as shown in Fig. 1. For the sake of simplicity, the quadrilateral operational characteristic was implemented for both phase and ground units (21P and 21G). Reactances of the 1st and 2nd zones were set, respectively, to 85% and 125% of the positive sequence reactance of the line, and the fault resistance coverage of both zones was set to 80 Ω [27].

External faults near TBT station were simulated (see the fault point shown in Fig. 1), considering initially the LCC-HVDC link is out of service. Figs. 9(a), 9(b), 9(c) and 9(d) depict the RX diagram with the impedance locus for solid faults AG, BC, BCG and ABC, respectively. As one can see, the impedance loci behaves as expected, settling at the 2nd zone. Conversely, Figs. 10(a), 10(b), 10(c) and 10(d) show the same RX diagrams, but now considering that both bipoles of the LCC-HVDC link are in service. In these cases, the voltage waveforms at AQD station are quite distorted, as well as the currents coming from the LCC-HVDC link. Since

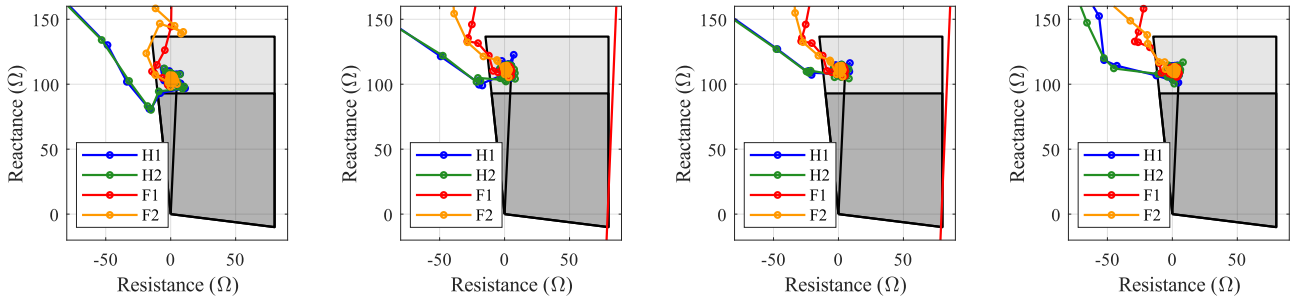

Fig. 9. RX diagram of the distance relay at AQD station for the evaluated external close-in faults (see the fault point shown in Fig. 1), considering the LCC-HVDC link is out of service: (a) AG; (b) BC; (c) BCG; (d) ABC.

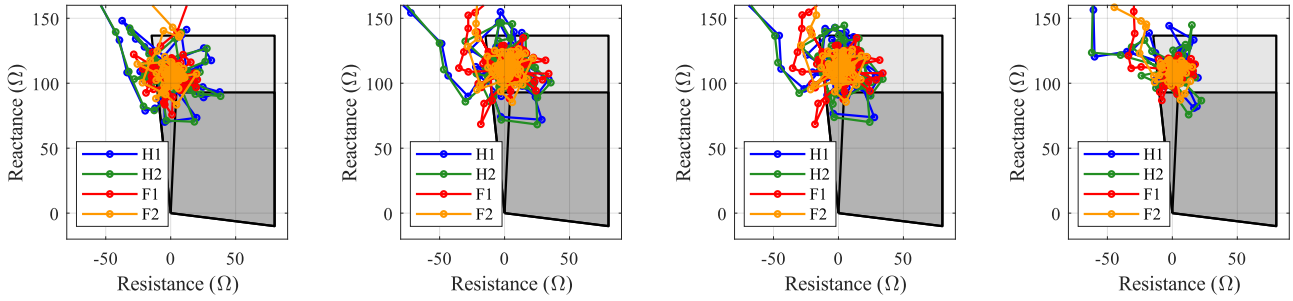

Fig. 10. RX diagram of the distance relay at AQD station for the evaluated external close-in faults (see the fault point shown in Fig. 1), considering the LCC-HVDC link is in service: (a) AG; (b) BC; (c) BCG; (d) ABC.

those currents are added to infeed currents from the AC lines and transformers connected to AQD station, errors on phasor estimation arise, leading the 1st distance zone to overreach the evaluated external faults. Moreover, as aforementioned, since half-cycle phasor estimation algorithms have poorer performance during CFs, they lead to a 1st zone overreach even more pronounced. Consequently, a false trip command may be issued, resulting in loss of selectivity of the protection system as a whole.

D. Line Differential Protection Function

To verify the performance of the transmission lines differential protection in the near vicinity of LCC-HVDC links, relays at both terminals of the line between AQD and TBT stations were considered (see relay points shown in Fig. 1). Phase and sequence differential elements were implemented by means of the $I_{op} \times I_{res}$ plane, being I_{op} the operating current and I_{res} the restraining current computed using phasors estimated by H1, H2, F1 and F2 algorithms as inputs. Line charging current and shunt reactor current compensation was carried out. The pick-up of differential elements was set to 0.1 per unit of the primary nominal current of CTs, whereas the slope was set to 0.3 taking into account CT errors [27].

Figs. 11(a), 11(b), 11(c) and 11(d) depict the $I_{op} \times I_{res}$ plane of 87L elements for solid external faults AG, BC, BCG and ABC, respectively (see the fault point shown in Fig. 1). In these cases, simulations were carried out with the LCC-HVDC link out of service. On the other hand, Figs. 12(a), 12(b), 12(c) and 12(d) show the same $I_{op} \times I_{res}$ planes, but considering that both bipoles of the LCC-HVDC link are in service. Once more, when distorted currents provided by the LCC-HVDC link are added, errors in phasor estimation arise, mainly for H1 and H2 algorithms. Notwithstanding, different from the distance protection function, in both evaluated cases, there would not occur false trip command issuing, ensuring the security of the differential scheme.

E. Directional Overcurrent Protection Function

Directional overcurrent elements have been widely used along with pilot schemes, such as permissive overreaching transfer trip (POTT), to provide unitary protection of transmission lines [27]. The impact of the LCC-HVDC links on these elements was assessed by simulating external faults near TBT station (see the fault point shown in Fig. 1). The pick-up of magnitude and minimum angle were set to 0.1 per unit and 10°, respectively [27]. Considering the POTT logic, 67 element at AQD station detects a forward fault and issues a permissive command. Conversely, if 67 element at TBT station detects a forward fault, the POTT scheme misoperates.

Figs. 13(a), 13(b), 13(c) and 13(d) depict the polar diagram of the zero sequence directional overcurrent element (67G) at TBT station for solid external faults AG, BC, BCG and ABC, respectively (see the fault point shown in Fig. 1), considering the LCC-HVDC link is out of service. Figs. 14(a), 14(b), 14(c) and 14(d), in turn, represent the same polar diagrams, but considering that both bipoles of the LCC-HVDC link are in service. As one can see, despite phasor estimation errors, the

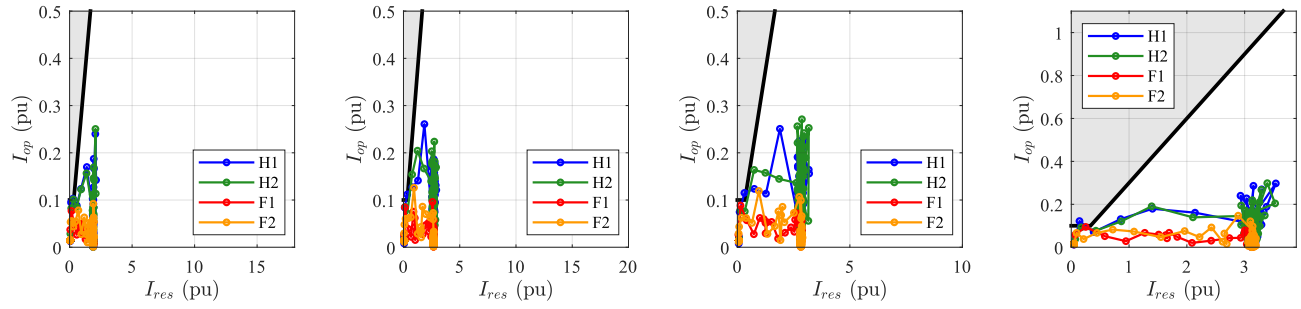

Fig. 11. $I_{op} \times I_{res}$ plane of the relay at AQD station for the evaluated external close-in faults (see the fault point shown in Fig. 1), considering the LCC-HVDC link is out of service: (a) AG; (b) BC; (c) BCG; (d) ABC.

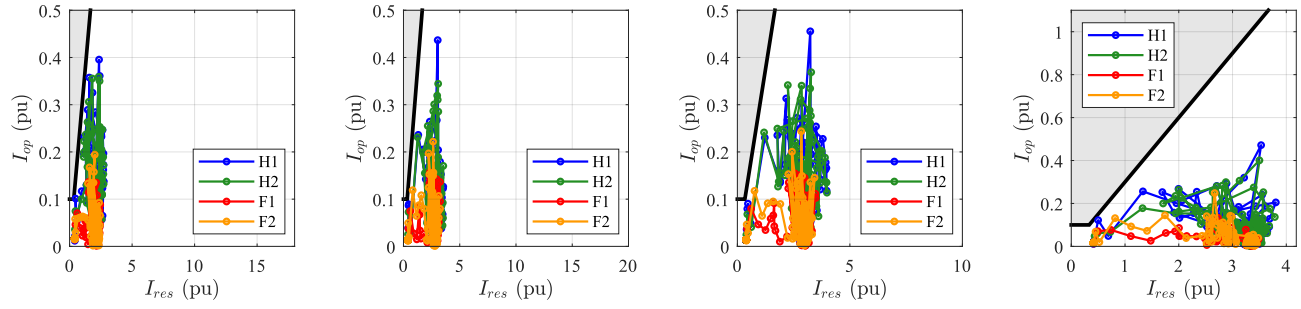

Fig. 12. $I_{op} \times I_{res}$ plane of the relay at AQD station for the evaluated external close-in faults (see the fault point shown in Fig. 1), considering the LCC-HVDC link is in service: (a) AG; (b) BC; (c) BCG; (d) ABC.

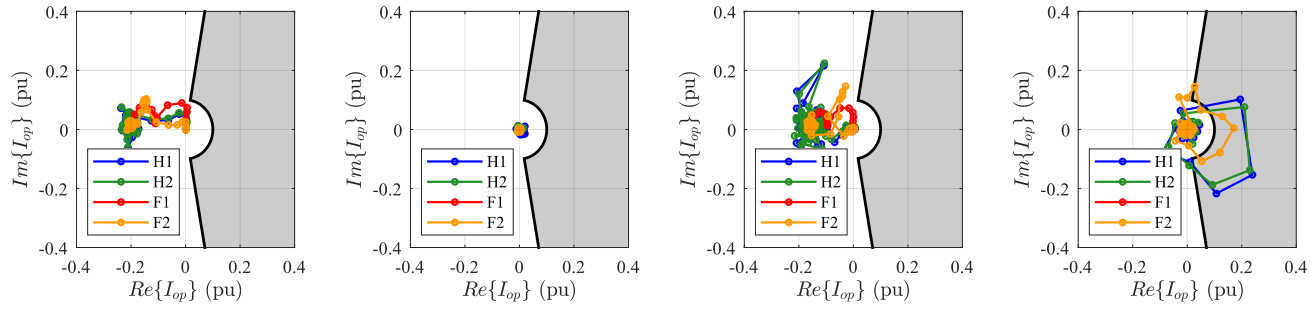

Fig. 13. Polar diagram of 67G element at TBT station for the evaluated external close-in faults (see the fault point shown in Fig. 1), considering the LCC-HVDC link is out of service: (a) AG; (b) BC; (c) BCG; (d) ABC.

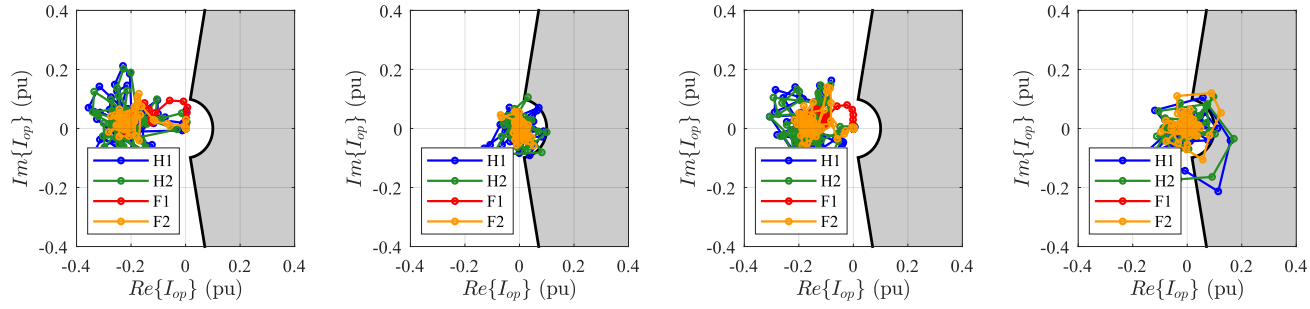

Fig. 14. Polar diagram of 67G element at TBT station for the evaluated external close-in faults (see the fault point shown in Fig. 1), considering the LCC-HVDC link is in service: (a) AG; (b) BC; (c) BCG; (d) ABC.

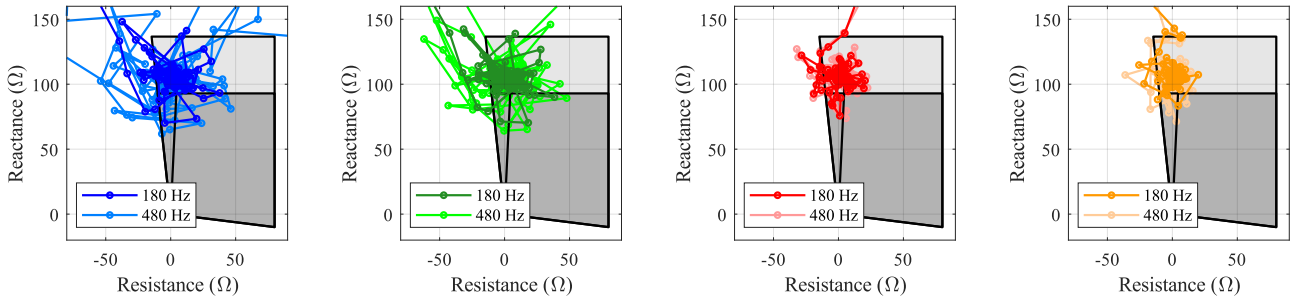

Fig. 15. RX diagram of the distance relay at AQD station for the evaluated AG close-in fault (see the fault point shown in Fig. 1), considering different cut-off frequencies for the third order low-pass anti-aliasing Butterworth filter: (a) H1 algorithm; (b) H2 algorithm; (c) F1 algorithm; (d) F2 algorithm.

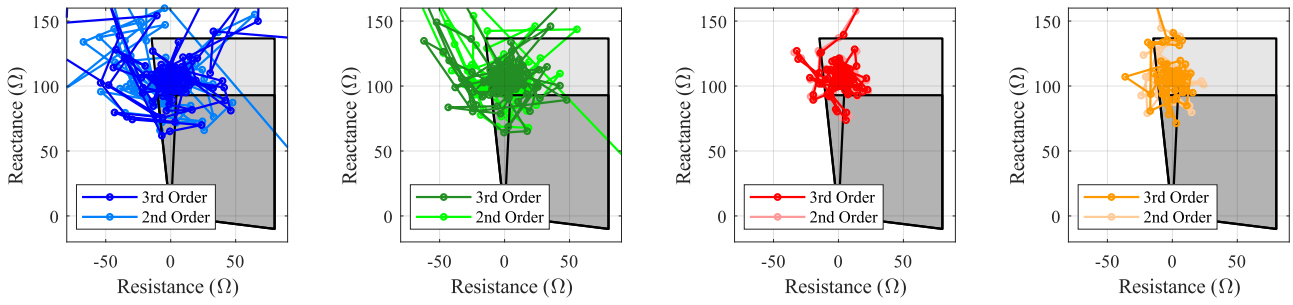

Fig. 16. RX diagram of the distance relay at AQD station for the evaluated AG close-in fault (see the fault point shown in Fig. 1), considering different orders for the low-pass anti-aliasing Butterworth filter with cut-off frequency at 480 Hz: (a) H1 algorithm; (b) H2 algorithm; (c) F1 algorithm; (d) F2 algorithm.

67G directional element at TBT station see a reverse fault for the AG and BCG faults as expected, because they are ground faults behind the relay. However, some points of the BC and ABC evaluated fault erroneously enter within the operation area, specially when the half-cycle algorithms H1 and H2 are used. As a result, POTT scheme may fail depending on the considered settings, requiring special countermeasures to provide secure directional sequence elements in the case of ungrounded faults. Furthermore, it is important to mention that 67G elements must not operate for phase-to-phase and three-phase faults, but they may misoperate because of the errors in phasor estimation process.

F. Impact of the Anti-Aliasing Filter

During sampling process, anti-aliasing filter plays a major role. On its design, two main settings are required: the order and the cut-off frequency [9]. The order is related to the quality factor (or Q-factor) of the filter, such that the larger it is, the larger the Q-factor, improving high-frequency components rejection. Notwithstanding, the larger is the order, the large the time delay on filtered signals, what is usually avoided in protection applications. The cut-off frequency is also related to the Q-factor, but it defines the center of the transition band and must be chosen in accordance with the Nyquist criteria [28]. As one can see, the combination of these two settings defines how selective is the filter, but also affects its time response. Furthermore, the combination of the anti-aliasing filter and phasor estimation algorithm governs the filtering process selectivity as a whole. Therefore, the impact of chosen filter order and cut-off frequency on phasor estimation and, in turn, on protection performance during CFs is evaluated in this paper. In order to do that, the distance protection function is once more assessed.

In Figs. 15(a), 15(b), 15(c) and 15(d) it is shown the distance protection performance for the close-in external solid AG fault (see the fault point shown in Fig. 1) for each evaluated phasor estimation algorithm, considering the third order low-pass anti-aliasing Butterworth filter with cut-off frequency at 180 Hz and 480 Hz. As one can see, half-cycle algorithms are more affected than full-cycle ones, depending on the cut-off frequency of the filter. Indeed, the large it is, the more H1 and H2 algorithms are affected, because the side-lobes on their frequency responses are less attenuated.

In Figs. 16(a), 16(b), 16(c) and 16(d) it is depicted the distance protection performance for the close-in external solid AG fault (see the fault point shown in Fig. 1) for each evaluated phasor estimation algorithm, considering the low-pass anti-aliasing Butterworth filter with cut-off frequency at 480 Hz and different orders. It can be seen that half-cycle algorithms are more affected than full-cycle ones. Indeed, the smaller is the filter order, the more H1 and H2 algorithms are affected, because the anti-aliasing filter Q-factor is reduced, leading side-lobes of their frequency responses to become less attenuated.

IV. Conclusions

The protection assessment of AC lines nearby LCC-HVDC links was presented. The major conclusions are presented next:

- CFs cause distortion on voltage and current waveforms of nearby AC system, leading to phasor estimation errors.
- Half-cycle algorithms suffer more from inaccuracies than full-cycle ones when quite distorted signals are evaluated, revealing the use of short windows may be an issue for protection schemes in these scenarios. Indeed, the smaller the data window is, the poorer is the performance of the algorithm when quite distorted signals are evaluated.
- Zone 1 of distance relays may misoperate, overreaching close-in externals faults. To overcome this drawback, the zone 1 reach can be reduced, but since the impedance locus may be unpredictable, a more conservative approach could be the zone 1 deactivation. For simplicity, quadrilateral characteristic was evaluated for both phase and ground distance units, but similar results would be obtained with the mho characteristic.
- 87L elements implemented through $I_{op} \times I_{res}$ plane operated correctly, preventing false trip for external faults. Negative and zero sequence differential elements (87LQ and 87LG) also performed correctly, but their results were not shown in this paper.
- 67G element operated correctly most of time. Nevertheless, for phase-to-phase and three-phase faults it may fail, compromising the POTT scheme. The same results were observed with the negative sequence element (ANSI code 67Q) for three-phase faults. Therefore, it is recommended not choosing small pick-up values.

It is noteworthy to point out that one can understand results reported in this paper as not being general, because they depend on different parameters such as system configuration, HVDC control strategies, load profile and fault conditions. Indeed, as aforementioned, CFs always cause phasor estimation errors, but not necessarily these errors lead protection to misoperate. Nevertheless, since the obtained results reveal that false trip command may be issued in some cases, an in-depth analysis is required to ensure security of the protection system as a whole. Therefore, this paper can be seen as the first step on this goal, such that further analysis will be presented in future works to support protection engineers during relays setting procedures of AC lines in the vicinity of LCC-HVDC systems.

REFERENCES

[1] E. W. Kimbark, *Direct current transmission*. Portland, USA: John Wiley & Sons Inc, 1971, vol. 1.

[2] E. Rahimi, A. M. Gole, J. B. Davies, I. T. Fernando, and K. L. Kent, "Commutation failure analysis in multi-infeed hvdc systems," *IEEE Transactions on Power Delivery*, vol. 26, no. 1, pp. 378–384, 2011.

[3] *Impact of hvdc stations on protection of ac systems*, CIGRE, WG B5/B4.25, 2011.

[4] P. Zhang, H. Li, G. Wang, and G. Zhu, "The impact of hvdc commutation failure on the distance protection," in *2010 Asia-Pacific Power and Energy Engineering Conference*, 2010, pp. 1–4.

[5] S. Huang, H. Shen, B. Fei, and O. Li, "Effect of commutation failure on the distance protection and the countermeasures," *IET Generation, Transmission Distribution*, vol. 9, no. 9, pp. 838–844, 2015.

[6] K. Li, R. Zhu, J. Li, F. Shi, W. Zhang, J. Wang, M. Liu, and G. Zhang, "The analysis of influence of hvdc commutation failure on distance protection," in *2019 IEEE 3rd Information Technology, Networking, Electronic and Automation Control Conference (ITNEC)*, 2019, pp. 578–582.

[7] K. Li, L. Ma, M. Liu, F. Shi, W. Zhang, J. Wang, C. Yang, and G. Zhang, "The analysis of influence of hvdc commutation failure on current differential protection," in *2018 2nd IEEE Conference on Energy Internet and Energy System Integration (EI2)*, 2018, pp. 1–5.

[8] Qiang Liu, Zexiang Cai, Minghui Huang, Zhiyao Liu, Yiquan Li, Xiaohua Li, and Lin Zhu, "Influence of hvdc commutation failure on directional comparison pilot protection of ac system," in *2008 Third International Conference on Electric Utility Deregulation and Restructuring and Power Technologies*, 2008, pp. 1943–1948.

[9] A. G. Phadke and J. S. Thorp, *Computer Relaying for Power Systems*, 2nd ed. New York, USA: John Wiley & Sons Inc, 2009.

[10] E. O. Schweitzer and D. Hou, "Filtering for protective relays," Schweitzer Engineering Laboratories, Pullman, USA, Tech. Rep., 1993.

[11] D. G. Hart, D. Novosel, and R. A. Smith, "Modified cosine filters," U.S. Patent 6,154,687, Nov. 2000.

[12] J.-C. Gu and S.-L. Yu, "Removal of dc offset in current and voltage signals using a novel fourier filter algorithm," *IEEE Transactions on Power Delivery*, vol. 15, no. 1, pp. 73–79, Jan. 2000.

[13] S.-L. Yu and J.-C. Gu, "Removal of decaying dc in current and voltages signals using a mofied fourier filter algorithm," *IEEE Transactions on Power Delivery*, vol. 16, no. 3, pp. 372–379, Jul. 2001.

[14] E. Rosolowski, J. Iżykowski, and B. Kasztenny, "Adaptive measuring algorithm suppressing a decaying dc component for digital protective relays," *Electric Power Systems Research*, vol. 60, pp. 99–105, Sep. 2001.

[15] T. S. Sidhu, X. Zhang, F. Albasri, and M. S. Sachdev, "Discrete-fourier-transform-based technique for removal of decaying dc from phasor estimates," *IEE Proceedings in Generation, Transmission and Distribution*, vol. 150, no. 6, pp. 745–752, Nov. 2003.

[16] Y. Guo, M. Kezunovic, and D. Chen, "Simplified algorithms for removal of the effect of exponentially decaying dc-offset on the fourier algorithm," *IEEE Transactions on Power Delivery*, vol. 18, no. 3, pp. 711–717, Jul. 2003.

[17] C.-S. Chen, C.-W. Liu, and J.-A. Jiang, "Application of combined adaptive fourier filtering technique and fault detector to fast distance protection," *IEEE Transactions on Power Delivery*, vol. 21, no. 2, pp. 619–626, Apr. 2006.

[18] S.-H. Kang, D.-G. Lee, S.-R. Nam, P. A. Crossley, and Y.-C. Kang, "Fourier transform-based modified phasor estimation method immune to the effect of the dc offsets," *IEEE Transactions on Power Delivery*, vol. 24, no. 3, pp. 1104–1111, Jul. 2009.

[19] K. M. Silva and B. F. Küsel, "Dft based phasor estimation algorithm for numerical digital relaying," *Electronics Letters*, vol. 49, no. 6, 2013.

[20] M. R. D. Zadeh and Z. Zhang, "A new dft-based current phasor estimation for numerical protective relaying," *IEEE Transactions on Power Delivery*, vol. 28, no. 4, pp. 2172–2179, Oct. 2013.

[21] K. M. Silva and F. A. O. Nascimento, "Modified dft-based phasor estimation algorithms for numerical relaying applications," *IEEE Trans. on Power Delivery*, vol. 33, no. 3, pp. 1165–1173, Jun. 2018.

[22] G. Luz, D. S. Jr, and S. G. Jr, "HVDC transmission line modeling analysis in PSCAD and ATP programs," *XIII Symposium of Specialists in Electric Operational and Expansion Planning*, pp. 1–6, 2014.

[23] "ATPDraw," https://www.atpdraw.net/, accessed: 2021-02-28.

[24] *ATP - Alternative Transient Program*, Leuven EMTP Center, Herverlee, Belgium, 1987.

[25] *EMTP Reference Models for Transmission Line Relay Testing*, IEEE Power System Relaying Committee, 2004. [Online]. Available: http://www.pes-psrc.org

[26] E. Pajuelo, G. Ramakrishna, and M. S. Sachdev, "Phasor estimation technique to reduce the impact of coupling capacitor voltage transformer transients," *IET Generation, Transmission & Distribution*, vol. 2, no. July 2007, pp. 588–599, 2008.

[27] S. H. Horowitz and A. G. Phadke, *Power System Relaying*, 3rd ed. West Sussex, England: John Wiley & Sons Inc, 2008.

[28] W. Rebizant, J. Szafran, and A. Wiszniewski, *Digital Signal Processing in Power System Protection and Control*, 1st ed. London, UK: Springer, 2011.